A Magnetoplasmonic Imaging Agent for Copper(I) with Dual Response by MRI and Dark Field Microscopy

Evan A. Weitz,[†] Cutler Lewandowski,[†] Eric D. Smolensky,[†] Małgorzata Marjańska,[‡] and Valérie C. Pierre[†,*]

[†]Department of Chemistry, University of Minnesota, Minneapolis, Minnesota 55455, United States, and [‡]Center for Magnetic Resonance Research and Department of Radiology, University of Minnesota, Minneapolis, Minnesota 55455, United States

ABSTRACT We present the design and synthesis of a responsive magnetoplasmonic assembly for copper(I) which allows monitoring of the concentration of the metal both in three dimensions by magnetic resonance imaging and with high spatial resolution by dark field microscopy. The probe consists of azide-functionalized iron oxide nanoparticles 11.6 nm in diameter and acetylene-terminated gold nanoparticles 44 nm in diameter that form three-dimensional networks of intermingled magnetic and plasmonic nanoparticles in the presence of copper. This aggregation results in a decrease in longitudinal relaxivity, and an initial increase followed by a sharp decrease in transverse relaxivity, a change observable both by T_1- and T_2-weighted images, concomitantly with a decrease of surface plasmon resonance intensity.

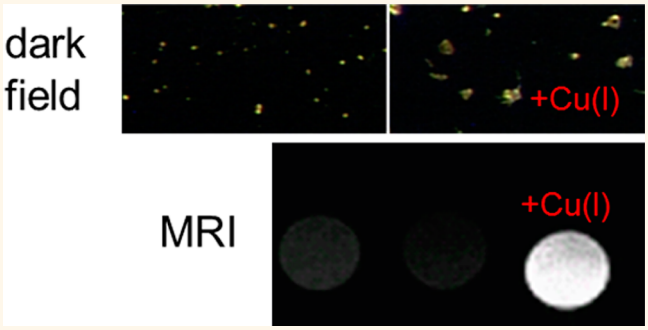

KEYWORDS: magnetic resonance imaging · dark field microscopy · iron oxide nanoparticle · gold nanoparticle · copper

Elevated levels and miscompartmentalization of copper is associated with several neurological disorders including Alzheimer's and Parkinson's diseases. In the case of Alzheimer's disease (AD), the nonspecific, adventitious binding of Cu(I) is implicated in the aggregation and damage of β amyloid and in the production of reactive oxygen species and high levels of oxidative stress.[1−3] Incomplete understanding of the bioinorganic chemistry of copper in these prevalent diseases has spurred the development of novel responsive contrast agents for Cu(I), which unfortunately have yet to be successfully translated to everyday *in vivo* imaging.[4−7] Desired attributes that current probes lack include both *in vivo* and high resolution imaging of the metal with a dynamic sensitivity relevant to its extracellular concentration in the brain in both healthy (1−10 μM) and diseased states (400 μM).[2] The three-dimensional deep-tissue imaging capabilities of magnetic resonance imaging (MRI) have rendered it the method of choice for *in vivo* imaging of the localization of biomarkers such as copper and plaques in the brains of animal models of AD.[8] In such studies, the contrast agent is delivered past the blood brain barrier either by direct intracranial injection, or by ultrasound or hyperosmotic shock-mediated delivery. The drawback of the poor spatial resolution of MRI can then be overcome by combining it with dark field microscopy, a technique with nanometer resolution that would enable precise localization of copper in plaques and subcellular compartments in brain slices previously selected from the MR images. Although such an approach could not be used for diagnostic purposes, it could prove a powerful tool to study the bioinorganic chemistry of copper directly in animal models. It first requires, however, the development of a *responsive* multimodal magnetoplasmonic probe. Herein we report a responsive magnetoplasmonic probe for dual imaging of Cu(I) by MRI and dark field microscopy.

Magnetoplasmonic agents are comprised of both magnetic iron oxide nanoparticles (MIONs), which display the high transverse relaxivity, r_2, needed for MRI, and gold

* Address correspondence to pierre@umn.edu.

Received for review February 22, 2013 and accepted June 8, 2013.

Published online June 08, 2013
10.1021/nn400928z

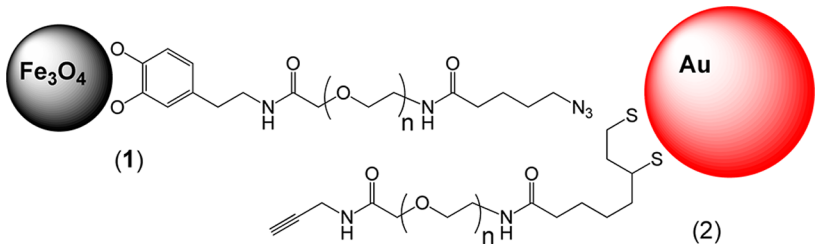

Figure 1. Chemical structures of the dual component responsive magnetoplasmonic probe for Cu(I): Fe_3O_4@Dop-PEG-N_3 (1) and Au@S_2−PEG-C≡CH (2).

nanoparticles, which provide the strong surface plasmon resonance (SPR) required for dark field microscopy. Typically, these are assembled in a single probe either *via* the synthesis of core−shell structures[9−12] or *via* the assembly of arrayed core−satellite systems.[13−15] Neither of these architectures, however, is suitable in the design of a dual responsive probe.

Responsive SPR behavior of gold nanoparticles and relaxivity of MIONs both rely on analyte-triggered aggregation of the metallic crystals. Previous studies have determined that a response in the SPR requires the gold nanoparticles to be >40 nm in diameter.[16] The need to maintain the superparamagnetism of MIONs limits their size to <20 nm.[17] For synthetic reason, combining the two materials in a single nanostructure is best achieved by keeping the MION at the center of the assembly. The required thick gold layer needed for SPR then has two main drawbacks: it reduces the magnetism and the relaxivities of the MION core,[18] and it maintains a large distance of at least 40 nm between MION crystals in the aggregated state. Maximum inter-particle magnetic interaction and thus maximum MR response, however, requires the MIONs to be less than 7 nm apart in the aggregated state.[19] These assemblies are therefore not suitable for the development of dual responsive probes as their MR response would be insufficient.

With this in mind, we have instead designed our dual responsive magnetoplasmonic agent to employ two independent water-stable dispersions of iron oxide and gold nanoparticles (Figure 1). The iron oxide nanoparticles which are used as MR probes are 11.7 nm in diameter. They are functionalized with azide-terminated polyethylene glycol anchored on the iron *via* strong catechol ligands, which affect neither the magnetism nor the relaxivity of the nanoparticles.[20] The SPR signal originates from separate gold nanoparticles, 44 nm in diameter, which are stabilized with polyethylene glycol (PEG) terminated with an acetylene using well-established thiol anchoring chemistry. Copper(I)-catalyzed Huisgen cycloaddition of the acetylene on the gold nanoparticles and the azides tethered to the MIONs leads to the formation of a three-dimensional assembly where the iron oxide and gold nanoparticles are intermingled (Figure 2). Aside from its ease of synthesis, this approach has the distinct

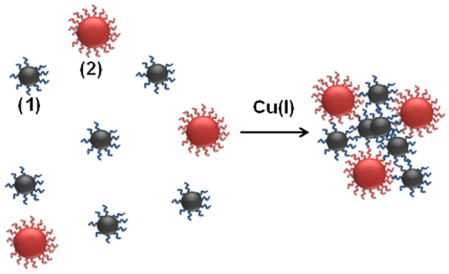

Figure 2. Proposed mode of action of our responsive magnetoplasmonic agent. Cu(I)-catalyzed Huisgen cycloaddition conjugates and intermingles the MIONs (1) and the gold nanoparticles (2) resulting in large clusters with varying r_1, r_2 and SPR signal.

advantage over other magnetoplasmonic assemblies that in the aggregated state, and in that state only, the iron oxide crystals are in close proximity to each other (<7 nm) as required to obtain maximum response.[19] To the best of our knowledge, this is the first example of a magnetoplasmonic agent that displays a responsive behavior in two different modalities. Note that the size of the nanoparticles, and the size of the clusters formed (<800 nm) are substantially smaller than the size of senile plaques characteristic of Alzheimer's disease. In humans, senile plaques are extracellular aggregate ranging in size between 10 and 120 μm in diameter, with the majority between 10 and 40 μm.[21] Magnetic and plasmonic nanoparticles therefore remain small enough to infiltrate plaques and detect copper, although it should be noted that this approach will enable detection of only the loosely bonded copper.

RESULTS AND DISCUSSION

Synthesis. The azide-terminated pegylated iron oxide nanoparticles Fe_3O_4@Dop-PEG-N_3 were synthesized as previously reported.[5] The thiol and acetyl terminated polymer was synthesized in a similar fashion from the commercial NHS-activated and BOC-protected PEG according to Scheme 1. In a first step, the acetylene functionality was added upon reaction with propargylamine. BOC deprotection enabled subsequent coupling with lipoic acid using a standard peptide coupling protocol. Reduction of the disulfide immediately prior to functionalization on the gold nanoparticles yielded the plasmonic part of the dual

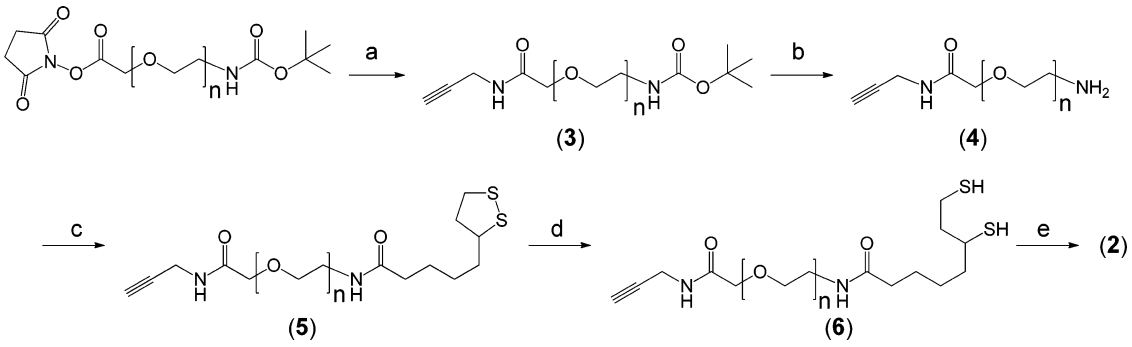

Scheme 1. Synthesis of AuNP@S_2—PEG-C≡CH (1). Reagents and conditions: (a) propargylamine, $CHCl_3$, DIPEA, RT, 48 h; (b) HCl (*aq*), 40 °C, 72 h; (c) lipoic acid, HATU, DMA, RT, 15 h; (d) DTT, H_2O, RT, 2 h; (e) Au nanoparticles, RT, 12 h.

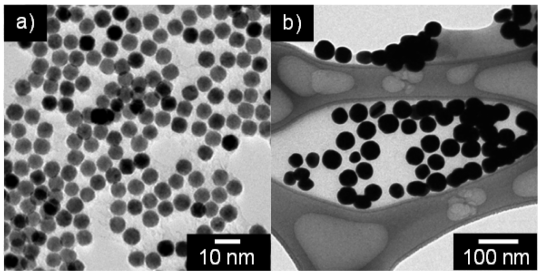

Figure 3. TEM images of (a) Fe_3O_4@Dop-PEG-N_3 (1) and (b) Au@S_2—PEG-C≡CH (2). Sizes of metallic crystals were determined to be 11.6 ± 0.7 and 44 ± 5 nm, respectively.

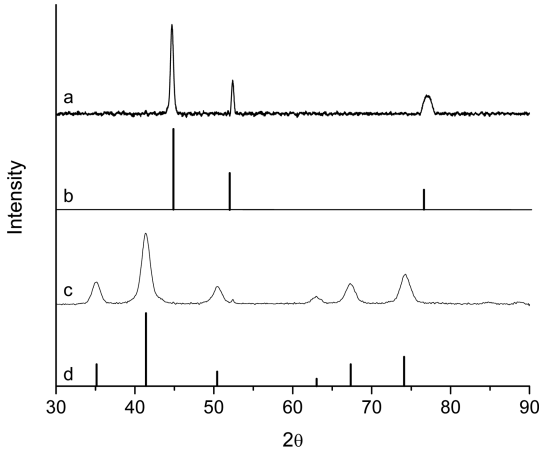

Figure 4. XRD spectra of (a) 44 nm Au@S_2—PEG-C≡CH (2), (b) reference pattern for Au (JCPDS #89-3697), (c) 11 nm Fe_3O_4@Dop-PEG-N_3 (1), and (d) reference pattern for magnetite (JCPDS #19-0629). Crystallite sizes, as calculated from the Scherrer equation, were determined to be 46 and 12 nm, respectively, in good agreement with the sizes determined by TEM analysis, indicating the particles are predominantly monocrystalline in nature.

responsive probe. The inorganic crystal cores of the azide-terminated magnetite nanoparticles and acetylene-coated gold nanoparticles were determined to be 11.6 ± 0.7 and 44 ± 5 nm in diameter, respectively, by transmission electron microscopy (TEM) (Figure 3). These sizes were selected so as to obtain maximal magnetic and plasmonic responses. Successful functionalization of the nanoparticles without alteration

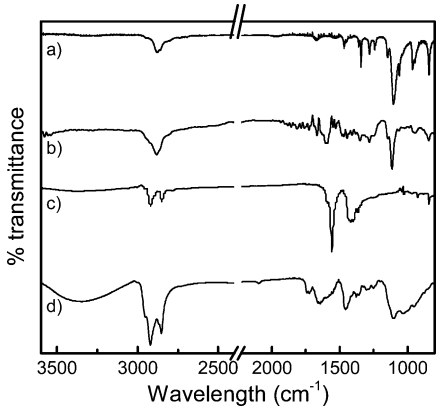

Figure 5. IR spectra of (a) S_2—PEG-C≡CH, (b) Au@S_2—PEG-C≡CH (2), (c) Fe_3O_4@OA, (d) Fe_3O_4@Dop-PEG-N_3 (1).

of their metallic structure was determined by powder X-ray diffraction (Figure 4) and IR spectroscopy (Figure 5).

Magnetic response: Relaxivity and MRI. The kinetic response of the transverse and longitudinal relaxivities of the probe to varying concentrations of Cu(I) is shown in Figure 6. The results are analogous to those observed with a purely iron oxide-based monomodal probe.[20] Although Cu(I) is a catalyst for the click reaction, regardless of the Cu(I) concentration both r_1 and r_2 plateau after 1 h of reaction. This observation likely results from the weak affinity of the PEG for the metal and leads to a stable, albeit nonlinear, response with increasing concentration of copper. Similar, noncatalytic behavior of the click reaction with copper was observed with other polymeric systems.[5] Advantageously, this concentration dependence enables us to monitor the concentration of copper.

As expected, Cu(I)-triggered aggregation of the gold and iron oxide nanoparticles decreases the longitudinal relaxivity, r_1, from 9.3 to 5.7 $mM^{-1}{}_{Fe}\ s^{-1}$ (Figure 7b). This result is comparable to that observed for our monomodal responsive contrast agent[5] and is in agreement with previous calculations by Gillis *et al.*[22] Aggregation of the gold and iron oxide nanoparticles separates the water molecules into two pools which

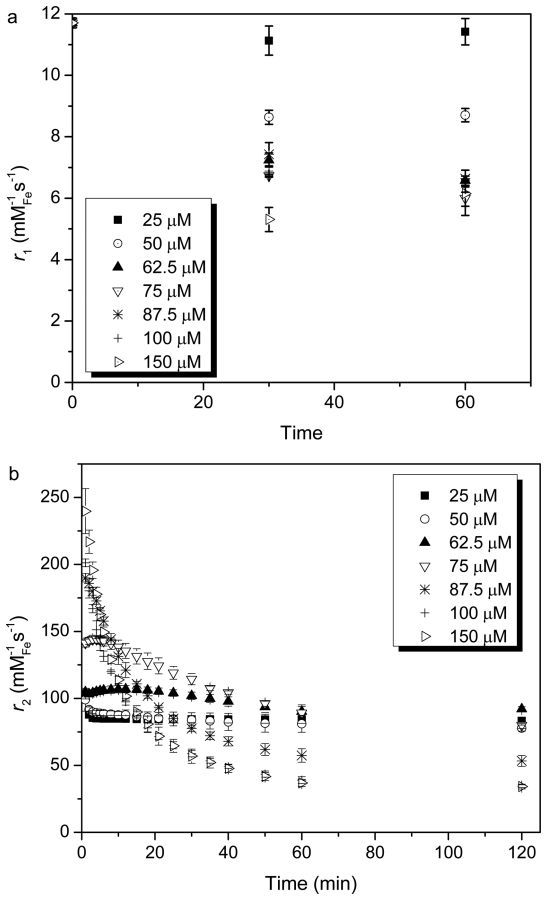

Figure 6. Kinetics of the response of (a) the longitudinal (r_1) and (b) the transverse (r_2) relaxivity of the probe for Cu(I). Experimental conditions: 1.5 T, 37 °C, water, pH 6, $[Fe]_{total}$ = 81.1 μM, $[Au]_{total}$ = 16.9 μM, [Cu(I)] = 25 μM (filled square), 50 μM (open circle), 62.5 μM (filled triangle), 75 μM (downward open triangle), 87.5 μM (star), 100 μM (cross), and 150 μM (left pointing open triangle), Cu(I) was generated *in situ* upon addition of sodium ascorbate from a stock solution of $CuSO_4$ (*aq*), [ascorbate] = 5 × [Cu(II)]. Error bars are standard deviation (n = 3).

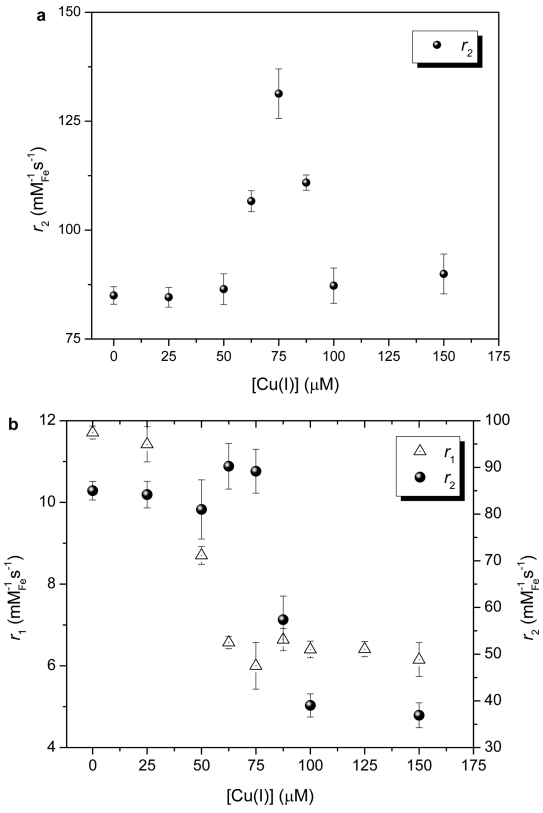

Figure 7. Decrease in longitudinal relaxivity (r_1, open triangles) and transverse relaxivity (r_2, filled circles) upon increase in Cu(I) concentration with (1) + (2) (a) after 15 min of reactions and (b) at equilibrium, after 2 h of reaction. Experimental conditions: 1.5 T, 37 °C, water, pH 7, $[Fe]_{total}$ = 81.1 μM, $[Au]_{total}$ = 16.9 μM, [ascorbate] = 3 × [Cu(I)]. Error bars are standard deviation (n = 3).

are exchanging at a rate slower than they are relaxing. Although the water molecules inside the cluster relax rapidly, the predominant bulk water outside the cluster relaxes slowly, such that the overall r_1 decreases.

Aggregation of the nanoparticles, on the other hand, does not necessarily yield a purely on/off response in terms of r_2, especially during the first 15 min of the reaction before the relaxivities plateaus. At 15 min, the transverse relaxivity increases with up to 62.5 μM Cu(I), then decreases with 100 μM copper (Figure 7a) . This observation is also in agreement both with previous results from our group[5] and with calculations from the Gillis group.[22] Importantly, the medium/high/low trend in r_2 is only observable at the beginning of the reaction. Once r_2 plateaus after 1 h of reaction, one observes a more linear on/off response (Figure 7b). Essentially, increase in r_2 upon nanoparticle clustering will be observed only when the rotational diffusion of the nanoparticles satisfies the motional averaging regime boundary condition, $\tau_D < 1/\Delta\omega_0$, where τ_D is the rotational diffusion of the nanoparticles and $\Delta\omega_0$ is the difference in frequency between bulk water molecules and those at the surface of the MIONs. While the condition is satisfied for monodispersed and slightly aggregated MIONs, this is not the case for clusters >300 nm in size for which a static dephasing regime is reached and r_2 decreases rapidly with increasing cluster size.[22] For the intended application of measuring copper concentration in plaques, the initial rise in r_2 with concentrations of copper between 50 and 75 μM at short reaction times are not relevant to clinical conditions. The extracellular copper concentration is either much below (<10 μM) for healthy brain or substantially above (>200 μM) in plaques. In our case, one therefore expects to see areas either of low T_2 (high r_2) where there are no plaques or high T_2 (low r_2) where there are plaques. However, the nonlinear response is a crucial problem with any responsive particulate contrast agents. It should not be assumed that nanoparticle-based responsive contrast agents always yield an off/on response with the presence of a plateau at high substrate concentrations. This behavior should be kept in mind when designing responsive particulate MRI contrast agents where monitoring of continuous concentrations of biomarkers is necessary.

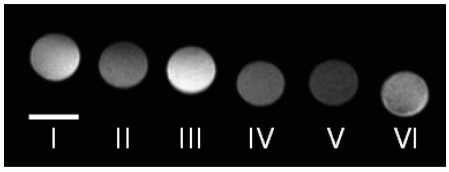

Figure 8. T_1-weighted gradient echo image of the probe in the absence and presence of Cu(I). (I) water; (II) (1); (III) (2); (IV) (1) + (2); (V) (1) + (2) + 150 μM Cu(I); (VI) (1) + (2) + 200 μM Cu(I). $[Fe]_{total}$ = 1 mM, $[Au]_{total}$ = 0.2 mM, reaction time = 16 h. 9.4 T, T_R = 11.15 ms, T_E = 5.59 ms, FOV: 15 mm × 15 mm, matrix: 256 × 256, slice thickness 1 mm, number of averages (na) = 4. Scale bar = 1 mm.

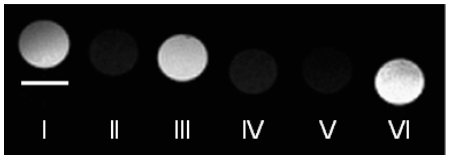

Figure 9. T_2-weighted spin echo image (I) water; (II) (1); (III) (2); (IV) (1) + (2); (V) (1) + (2) + 150 μM Cu(I); (VI) (1) + (2) + 200 μM Cu(I). $[Fe]_{total}$ = 1 mM, $[Au]_{total}$ = 0.2 mM, reaction time =16 h. 9.4 T, T_R = 2000 ms, T_E = 12.18 ms, FOV: 15 mm × 15 mm, matrix: 256 × 256, slice thickness 1 mm, na = 1. Scale bar = 1 mm.

T_1 and T_2-weighted MR images of the MION and gold nanoparticles in the presence and absence of Cu(I) at 9.4 T reproduce the trends measured by NMR at 1.5 T (Figures 8 and 9, respectively). In the absence of MIONs, no contrast is observed regardless of whether the gold nanoparticles are present or not (I and III). Similarly, in the absence of Cu(I), Fe_3O_4@Dop-PEG-N_3 darkens the phantom by the same amount regardless of the presence of gold nanoparticles (II and IV). When both components are present, low concentrations of Cu(I) aggregate the nanoparticles into small clusters that remain within the motional averaging regime boundary, r_2 increases, and the phantom darkens (V). Higher concentrations of Cu(I), however, yield larger clusters that fall in the static dephasing regime. As a result of r_2 decreasing, the phantom lightens and the contrast disappears (VI). Note that the same trend is observed in both T_1- and T_2-weighted images. The very short T_2* of MIONs negate any positive T_1 effect such that the contrast of T_1-weighted images is actually proportional to r_2 regardless of r_1. Do note that although the kinetic data were measured on an NMR at 1.5 T whereas the MRI phantoms were obtained at 9.4 T, the trends are unaffected by the strength of the magnetic field. Indeed, prior studies have determined that the transverse relaxivity of iron oxide nanoparticles remains constant above 0.5 T.[23] The longitudinal relaxivity, r_1, does decrease substantially between 1.5 and 9.4 T, but since contrast of T_1-weighted images of MION are primarily governed not by r_1 but by the very short T_2*, the decrease in r_1 with increasing magnetic field has little impact on the T_1-weighted gradient echo images.

Plasmonic Response: Dark Field Microscopy. Our probe was designed to respond both magnetically, with modulation of both r_1 and r_2, and optically, with changes in the SPR intensity and wavelength. As predicted from Mirkin's research,[16,24,25] the SPR signal is substantially attenuated upon addition of Cu(I); a 40% decrease upon addition of 300 μM of the metal is observed. As with the relaxivities, the amount of SPR quenching is steeply dependent on the concentration of copper (Figure 10). Surprisingly, the SPR band red shifts barely 5 nm, substantially less than typically observed.[16] Theoretical calculations have predicted that electronic coupling between gold nanoparticles is severely attenuated for interparticle distances greater than 2.5 times the diameter of the nanoparticles.[26] These calculations are in agreement with the observations of Liphardt *et al.* who reported that for 42 nm gold nanoparticle molecular rulers, the maximum change in λ_{SPR} is reached when the gold crystals are 20 nm apart.[27] For our probe, given the diameter of the gold and iron oxide crystals (44 and 11.7 nm,

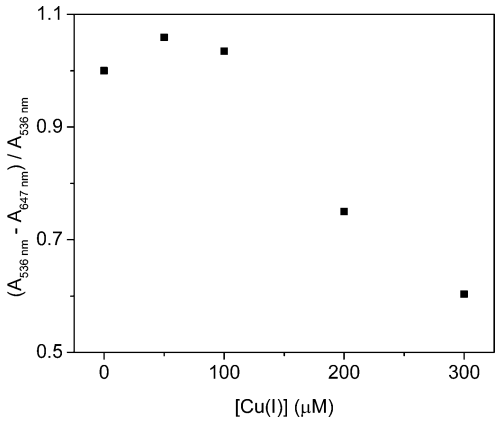

Figure 10. Relative intensity of the SPR absorbance band upon addition of Cu(I) to the magnetoplasmonic probe. Experimental conditions: 37 °C, water, pH 7, $[Fe]_{total}$ = 81.1 μM, $[Au]_{total}$ = 16.9 μM, [ascorbate] = 3 × [Cu(I)], reaction time =30 min.

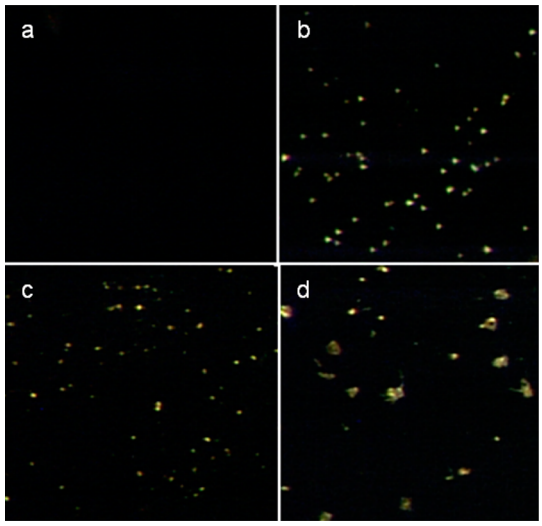

Figure 11. Dark field microscopy images of (a) (1), (b) (2), (c) (1) + (2), (d) (1) + (2) + 150 μM Cu(I)Asc, reaction time = 2 h.

respectively) and the thickness of the PEG coating (8 nm, as estimated from DLS measurements), the small shift in λ_{SPR} observed suggests a likely aggregation of multiple layers of MIONs between gold nanoparticles. A monolayer of MION would have separated the gold nanoparticles by *ca.* one time their diameter, which would have created a greater shift of λ_{SPR} than that observed.

The optical response of the probe to Cu(I)-induced clustering is directly observable at high resolution by dark-field microscopy (Figure 11). The smaller MIONs do not scatter light, nor do they affect the ability of gold nanoparticles to do so. After addition of Cu(I), the larger clusters appear bigger and scatter light with greater intensity, in accord with previous reports.[27] Notably, while the increase in cluster size is evident, the colorimetric response is negligible; the particles scatter green light irrespective of their aggregation. These observations are in complete agreement with the UV−visible results discussed above.

CONCLUSION

We report the synthesis and evaluation of a magnetoplasmonic probe with dual response to copper(I) by relaxivity and visible spectroscopy. Cu(I)-catalyzed cycloaddition of azide-functionalized MION with acetylene-coated gold nanoparticles causes a decrease in r_1 and an initial 2-fold increase, followed by a near-complete loss, of r_2. Of these changes, that in transverse relaxivity is more readily observable by both T_1- and T_2-weighted gradient-echo MRI. Clustering also quenches the SPR absorbance band of the probe, albeit with a negligible red-shift of λ_{SPR}. As a result, addition of Cu(I) to our probe results in larger clusters that appear bigger and brighter by dark field microscopy, but do not change in color.

METHODS

General. Unless otherwise noted, starting materials were obtained from commercial suppliers and used without further purification. Water was distilled and further purified by a Millipore cartridge system (resistivity 18 × 10^6 Ω). ^{1}H NMR spectra were recorded on a Varian 500 at 500 MHz or on a Varian 300 at 300 MHz at the Le Claire-Dow Characterization Facility of the Department of Chemistry of the University of Minnesota; the solvent residual peak was used as an internal reference. ^{1}H NMR data are reported as follows: chemical shift (δ, ppm), multiplicity (s, singlet; d, doublet; t, triplet; m, multiplet), integration, coupling constant (Hz). Mass spectra (LR = low resolution; HR = high resolution; ESI MS = electrospray ionization mass spectrometry) were recorded on a Bruker BioTOF II at the Waters Center for Innovation for Mass Spectrometry Facility at the Department of Chemistry at the University of Minnesota, Twin-Cities. TEM images were collected on a FEI Tecnai T12 at 120 kV. The hydrodynamic size of the particle aggregates was measured by Dynamic Light Scattering (DLS) with a 90Plus/BI-MAS particle size analyzer (Brookhaven Instruments Corporation). Solid state infrared spectra were recorded on a Thermo Nicolet 6700 FTIR using an ATR adapter. Data was collected between 700 and 3700 cm^{-1}. Relaxivities were measured at 37 °C and 1.5 T (60 MHz) on a Bruker Minispec mq60. UV−visible spectra were recorded on a Varian Cary 100 Biospectrophotometer. Dark field microscopy images were obtained on a Nikon Optishot-Pol microscope.

Fe_3O_4@Dop-PEG-N_3 (1). Fe_3O_4@Dop-PEG-N_3 (**1**) nanoparticles were synthesized as previously reported.[5] Successful synthesis was established by ^{1}H NMR spectroscopy, LR ESI MS, and IR spectroscopy.

BOC-PEG-C≡CH (3). BOC-NH-PEG-NHS ester (200 mg, 0.100 mmol) was dissolved in dry CH_2Cl_2 (25 mL) and magnetically stirred under argon. Propargylamine (19.2 μL, 0.300 mmol) and *N*,*N*-diisopropylethylamine (97.7 μL, 0.600 mmol) were then added, and the reaction mixture was gently refluxed for 46 h. Volatiles were removed under reduced pressure yielding a yellow oil that was redissolved in mQ H_2O (1.5 mL) and purified *via* NAP-5 column (eluent: 1 mL H_2O) before being lyophilized to yield the acetylene-terminated polymer **3** as a white solid (172 mg, 88.6%). ^{1}H NMR (300 MHz, $CDCl_3$) δ 7.43 (br s, 1 H), 5.05 (br s, 1 H), 4.10 (dd, J_1 = 5.7 Hz, J_2 = 2.7 Hz, 2 H), 4.02 (s, 2 H), 3.74−3.52 (m, PEG H), 3.31 (t, J = 4.5 Hz, 1 H), 2.24 (t, J = 2.4 Hz, 1 H), 1.44 (s, 9 H). ^{13}C NMR (75 MHz, $CDCl_3$) δ 170.6, 156.6, 80.4, 79.7, 78.1, 72.5−69.9 (m, $-CH_2CH_2O-$), 41.0, 29.1, 29.0. HRMS-ESI (*m*/*z*) $[M + 2\,Na]^{2+}$ calc for $C_{104}H_{204}N_2O_{50}$: 1164.1650; found, 1164.1689; error, 3.35 ppm.

NH_2−PEG-C≡CH (4). The protected polymer **3** (86.0 mg, 44.3 μmol) was dissolved in dry $CHCl_3$ (5 mL) and magnetically stirred in an ice bath. Trifluoroacetic acid (10 mL) was added dropwise over 3 min, and the reaction mixture was allowed to warm to ambient temperature and stirred for 18 h. Volatiles were removed under reduced pressure yielding a colorless oil that was redissolved in cold MeOH (5 mL) and concentrated again yielding the amine **4** as a colorless oil (81.1 mg, ≥ 99%). ^{1}H NMR (300 MHz, $CDCl_3$) δ 7.51 (br s, 1 H), 4.10 (dd, J_1 = 5.7 Hz, J_2 = 2.4 Hz, 2 H), 4.04 (s, 2 H), 3.89 (br s, 2 H), 3.81−3.57 (m, PEG H), 3.41 (t, J = 4.5 Hz, 2 H), 3.20 (br s, 2 H), 2.25 (t, J = 2.4 Hz, 1 H). ^{13}C NMR (75 MHz, $CDCl_3$) δ 162.1, 79.1, 71.6, 70.1, 69.6−69.0 (m, $-CH_2CH_2O-$), 66.0, 38.8, 27.9. HRMS-ESI (*m*/*z*) $[M + H + Na]^{2+}$ calc for $C_{99}H_{197}N_2O_{48}$: 1103.1478; found, 1103.1434; error, 3.99 ppm.

S−S−PEG-C≡CH (5). Lipoic acid (18.5 mg, 90.1 μmol) was dissolved in dry DMF (10 mL) and magnetically stirred. HATU (2-(7-Aza-1*H*-benzotriazole-1-yl)-1,1,3,3-tetramethyluronium hexafluorophosphate, 68.4 mg, 180 μmol) was then added and the reaction mixture was stirred for 35 min at ambient temperature. A solution of the amine-terminated **S2** (60.0 mg, 32.6 μmol) in dry DMF (10 mL) was then added, followed by *N*,*N*-diisopropylethylamine (64.0 μL, 360 μmol). The reaction mixture was stirred overnight at ambient temperature and then concentrated under reduced pressure yielding a brown oil, which was redissolved in mQ H_2O (1.0 mL) and purified *via* NAP-5 column (eluent: 1.0 mL H_2O) and lyophilized yielding the disulfide **5** as a white solid (42.2 mg, 63.5%). ^{1}H NMR (300 MHz, $CDCl_3$) δ 7.43 (br s, 1 H), 6.26 (br s, 1 H), 4.01 (dd, J_1 = 5.7 Hz, J_2 = 2.4 Hz, 2 H), 3.94 (s, 2 H), 3.80 (t, J = 5.4 Hz, 2 H), 3.67−3.46 (m, PEG H), 3.12−3.02 (m, 3 H), 2.38 (hextet, J = 6.6 Hz, 1 H), 2.19 (t, J = 2.4 Hz, 1 H), 2.12 (t, J = 7.2 Hz, 2 H), 1.83 (hextet, J = 6.6 Hz, 1 H), 1.66−1.52 (m, 4 H). ^{13}C NMR (75 MHz, $CDCl_3$) δ 173.6, 162.1, 80.4, 78.0, 71.9, 71.1−70.7 (m, $-CH_2CH_2O-$), 70.4, 69.9, 57.1, 43.1, 40.9, 39.8, 39.1, 36.9, 35.3, 29.6, 28.9, 26.0. HRMS-ESI (*m*/*z*) $[M + H + K]^{2+}$ calc for $C_{103}H_{200}N_2O_{47}S_2$: 1161.1250; found, 1161.1294; error, 3.79 ppm.

S_2−PEG-C≡CH (6). The disulfide **5** (21.1 mg, 10.4 μmol) was dissolved in mQ H_2O (5 mL) and magnetically stirred. Dithiolthreitol (20 mg, 130 μmol) was added and the reaction mixture was stirred at ambient temperature for 2 h and then concentrated under reduced pressure, purified *via* NAP-5 column (eluent: 1.0 mL H_2O) yielding the dithiol **6** which was used immediately to functionalize gold nanoparticles.

Au@S_2−PEG-C≡CH (2). To the dithiol **S4** (9 mg, 4 μmol) in H_2O (1 mL) was added 500 μL of a solution of 50 nm gold nanoparticles ($[Au]_{tot}$ = 0.254 μM) and the reaction mixture was

gently stirred for 18 h. The pink reaction mixture was then centrifuged slowly yielding a pink pellet and the supernatant which was discarded. The pellet was then redissolved in mQ H_2O (2 mL) yielding **1** as a pink solution in H_2O.

Relaxivity. Longitudinal (T_1) and transverse (T_2) relaxation times of the nanoparticles in mQ water were measured on a Bruker Minispec mq60 NMR Analyzer at 60 MHz and 37 °C using the inversion recovery sequence and the Carr−Purcell−Meiboom−Gill sequence, respectively. The total concentration of iron of each sample was determined by the equation below. Briefly, 5.0 μL of each probe was suspended in 200 μL of HNO_3 (*aq*) and 100 μL of mQ water and further heated at 110 °C overnight. This treatment efficiently and completely decomposes the nanoparticles into metal aqua species. The concentration of iron in the final, strongly acidic media was then determined either by ICP-OES or by measuring T_1 of each sample using a calibration plot obtained from standard solutions of $FeCl_3$ in 2:1 HNO_3:mQ water (same media as that of the decomposed nanoparticles) previously calibrated by ICP OES. Note that the aqua gold species does not contribute to T_1, so the latter method enables rapid determination of only the iron concentration in a sample. Importantly, iron concentrations of samples determined by relaxivity and ICP-OES are within experimental errors.

Once the iron concentrations of each sample were determined, the longitudinal (r_1) and transverse (r_2) relaxivities were determined from the following equation.

$$r_i[\mathrm{Fe}] = \frac{1}{T_{i,\,\mathrm{obs}}} - \frac{1}{T_{i,\,\mathrm{H_2O}}}, \quad \text{where } i = 1, 2$$

Kinetic Relaxivity Studies. The nanoparticle probes (**1**) and (**2**) were suspended in mQ water at 37 °C and the relaxation times T_1 and T_2 were measured. Cu(I)ascorbate was then added to bring the final concentration of Cu(I) to 0, 25, 50, 62.5, 75, 87.5, 100, 150, and 200 μM. In each run, [ascorbate] = 5 × [Cu(I)]. The excess ascorbate is used in order to maintain all copper in its +1 oxidation state. Relaxation times T_1 and T_2 were recorded over the next 60 min after the addition of copper. All measurements were performed at 37 °C.

Magnetic Resonance Imaging. MR images were acquired using a 9.4-T, 31-cm horizontal bore magnet (Magnex Scientific, Oxford, U.K.) interfaced with a Varian Direct Drive console (Varian, Palo Alto, CA). The magnet was equipped with a gradient insert capable of reaching 450 mT/m in 200 μs (Resonance Research, Inc., Billerica, MA). The radiofrequency coil assembly consisted of a linear surface coil (12 mm diameter). Gradient echo images were acquired using following parameters: repetition time (T_R) = 11.15 ms, echo time (T_E) = 5.59 ms, FOV = 15 mm × 15 mm, matrix = 256 × 256, slice thickness = 1 mm, number of averages (na) = 4. Spin echo images were acquired using following parameters: T_R = 2 s, T_E = 12.18 ms, FOV = 15 mm × 15 mm, matrix = 256 × 128, slice thickness = 1 mm, na = 1.

Kinetic UV−Vis Studies. The nanoparticle probes (**1**) and (**2**) were suspended in a solution of mQ water at 20 °C and the absorbance spectra recorded between 250 and 800 nm. Cu(I)ascorbate was then added to bring the final concentration of Cu(I) to 0, 50, 100, 200, and 300 μM. In each run, [ascorbate] = 5 × [Cu(I)]. The excess ascorbate is used in order to maintain all copper in its +1 oxidation state. Absorbance spectra were recorded 30 min, 1 h, and 2 h after the addition of copper. All measurements were performed at 20 °C.

Conflict of Interest: The authors declare no competing financial interest.

Acknowledgment. This work was supported partially by the MRSEC Program of the National Science Foundation (DMR-0819885), and by the NCRR (P41 RR008079), the NIBIB (P41 EB015894) of the National Institutes of Health and the W. M. Keck Foundation. Part of this work was carried out in the College of Science and Engineering Characterization Facility, University of Minnesota, which has received capital equipment funding from the NSF through the MRSEC, ERC and MRI programs. E.D.S. gratefully acknowledges partial support from the NIH CBITG (GM 08700). We thank A. Massari for use of the infrared spectrometer. We thank Katie Hurley with assistance obtaining the XRD data.

REFERENCES AND NOTES

1. Gaggelli, E.; Kozlowski, H.; Valensin, D.; Valensin, G. Copper Homeostasis and Neurodegenerative Disorders (Alzheimer's, Prion, and Parkinson's Diseases and Amyotrophic Lateral Sclerosis). *Chem. Rev.* **2006**, *106*, 1995–2044.
2. Scott, L. E.; Orvig, C. Medicinal Inorganic Chemistry Approaches to Passivation and Removal of Aberrant Metal Ions in Disease. *Chem. Rev.* **2009**, *109*, 4885–4910.
3. Zheng, Z. Q.; White, C.; Lee, J.; Peterson, T. S.; Bush, A. I.; Sun, G. Y.; Weisman, G. A.; Petris, M. J. Altered Microglial Copper Homeostasis in a Mouse Model of Alzheimer's Disease. *J. Neurochem.* **2010**, *114*, 1630–1638.
4. Que, E. L.; Gianolio, E.; Baker, S. L.; Aime, S.; Chang, C. J. A Copper-Activated Magnetic Resonance Imaging Contrast Agent with Improved Turn-On Relaxivity Response and Anion Compatibility. *Dalton Trans.* **2010**, *39*, 469–476.
5. Smolensky, E. D.; Marjanska, M.; Pierre, V. C. A Responsive Particulate MRI Contrast Agent for Copper(I): A Cautionary Tale. *Dalton Trans.* **2012**, *41*, 8039–8046.
6. Que, E. L.; Chang, C. J. A Smart Magnetic Resonance Contrast Agent for Selective Copper Sensing. *J. Am. Chem. Soc.* **2006**, *128*, 15942–15943.
7. Que, E. L.; Gianolio, E.; Baker, S. L.; Wong, A. P.; Aime, S.; Chang, C. J. Copper-Responsive Magnetic Resonance Imaging Contrast Agents. *J. Am. Chem. Soc.* **2009**, *131*, 8527–8536.
8. Sosnovik, D. E.; Weissleder, R. Emerging Concepts in Molecular MRI. *Curr. Opin. Biotechnol.* **2007**, *18*, 4–10.
9. Smolensky, E. D.; Neary, M. C.; Zhou, Y.; Berquo, T. S.; Pierre, V. C. Fe3O4@Organic@Au: Core-Shell Nanocomposites with High Saturation Magnetisation as Magnetoplasmonic MRI Contrast Agents. *Chem. Commun.* **2011**, *47*, 2149–2151.
10. Zhang, M.; He, X.; Chen, L.; Zhang, Y. Preparation of Ida-Cu Functionalized Core-Satellite Fe3O4/Polydopamine/Au Magnetic Nanocomposites and Their Application for Depletion of Abundant Protein in Bovine Blood. *J. Mater. Chem.* **2010**, *20*, 10696–10704.
11. Zhou, X.; Xu, W.; Wang, Y.; Kuang, Q.; Shi, Y.; Zhong, L.; Zhang, Q. Fabrication of Cluster/Shell Fe3O4/Au Nanoparticles and Application in Protein Detection *via* a SERS Method. *J. Phys. Chem. C* **2010**, *114*, 19607–19613.
12. Leung, K. C. F.; Xuan, S. H.; Zhu, X. M.; Wang, D. W.; Chak, C. P.; Lee, S. F.; Ho, W. K. W.; Chung, B. C. T. Gold and Iron Oxide Hybrid Nanocomposite Materials. *Chem. Soc. Rev.* **2012**, *41*, 1911–1928.
13. Tian, J.; Zheng, F.; Zhao, H. Nanoparticles with Fe_3O_4−Nanoparticle Cores and Gold-Nanoparticle Coronae Prepared by Self-Assembly Approach. *J. Phys. Chem. C* **2011**, *115*, 3304–3312.
14. Zhang, H.; Zhong, X.; Xu, J. J.; Chen, H. Y. Fe_3O_4/Polypyrrole/Au Nanocomposites with Core/Shell/Shell Structure: Synthesis, Characterization, and Their Electrochemical Properties. *Langmuir* **2008**, *24*, 13748–13752.
15. Wang, L.; Bai, J.; Li, Y.; Huang, Y. Multifunctional Nanoparticles Displaying Magnetization and Near-IR Absorption. *Angew. Chem., Int. Ed.* **2008**, *47*, 2439–2442.
16. Hurst, S. J.; Hill, H. D.; Mirkin, C. A. "Three-Dimensional Hybridization" with Polyvalent DNA-Gold Nanoparticle Conjugates. *J. Am. Chem. Soc.* **2008**, *130*, 12192–12200.
17. Laurent, S.; Forge, D.; Port, M.; Roch, A.; Robic, C.; Elst, L. V.; Muller, R. N. Magnetic Iron Oxide Nanoparticles: Synthesis, Stabilization, Vectorization, Physicochemical Characterizations, and Biological Applications. *Chem. Rev.* **2008**, *108*, 2064–2110.
18. Wang, L.; Park, H.-Y.; Lim, S. I. I.; Schadt, M. J.; Mott, D.; Luo, J.; Wang, X.; Zhong, C.-J. Core@Shell Nanomaterials: Gold-Coated Magnetic Oxide Nanoparticles. *J. Mater. Chem.* **2008**, *18*, 2629–2635.
19. Frankamp, B. L.; Boal, A. K.; Tuominen, M. T.; Rotello, V. M. Direct Control of the Magnetic Interaction between Iron Oxide Nanoparticles through Dendrimer-Mediated Self-Assembly. *J. Am. Chem. Soc.* **2005**, *127*, 9731–9735.
20. Smolensky, E. D.; Park, H. Y. E.; Berquo, T. S.; Pierre, V. C. Surface Functionalization of Magnetic Iron Oxide Nanoparticles for MRI Applications - Effect of Anchoring Group

and Ligand Exchange Protocol. *Contrast Media Mol. Imaging* **2011**, *6*, 189–199.
21. Pinzer, B. R.; Cacquevel, M.; Modregger, P.; McDonald, S. A.; Bensadoun, J. C.; Thuering, T.; Aebischer, P.; Stampanoni, M. Imaging Brain Amyloid Deposition Using Grating-Based Differential Phase Contrast Tomography. *NeuroImage* **2012**, *61*, 1336–1346.
22. Roch, A.; Gossuin, Y.; Muller, R. N.; Gillis, P. Superparamagnetic Colloid Suspensions: Water Magnetic Relaxation and Clustering. *J. Magn. Magn. Mater.* **2005**, *293*, 532–539.
23. Smolensky, E. D.; Park, H.-Y. E.; Zhou, Y.; Rolla, G. A.; Marjanska, M.; Botta, M.; Pierre, V. C. Scaling Laws at the Nanosize: The Effect of Particle Size and Shape on the Magnetism and Relaxivity of Iron Oxide Nanoparticle Contrast Agents. *J. Mater. Chem. B* **2013**, *1*, 2818–2828.
24. Hill, H. D.; Hurst, S. J.; Mirkin, C. A. Curvature-Induced Base Pair "Slipping" Effects in DNA-Nanoparticle Hybridization. *Nano Lett.* **2009**, *9*, 317–321.
25. Hurst, S. J.; Hill, H. D.; Macfarlane, R. J.; Wu, J. S.; Dravid, V. P.; Mirkin, C. A. Synthetically Programmable DNA Binding Domains in Aggregates of DNA-Functionalized Gold Nanoparticles. *Small* **2009**, *5*, 2156–2161.
26. Su, K. H.; Wei, Q. H.; Zhang, X.; Mock, J. J.; Smith, D. R.; Schultz, S. Interparticle Coupling Effects on Plasmon Resonances of Nanogold Particles. *Nano Lett.* **2003**, *3*, 1087–1090.
27. Reinhard, B. M.; Siu, M.; Agarwal, H.; Alivisatos, A. P.; Liphardt, J. Calibration of Dynamic Molecular Rule Based on Plasmon Coupling between Gold Nanoparticles. *Nano Lett.* **2005**, *5*, 2246–2252.